Online-Journals.org

iJOE International Journal of Online and Biomedical Engineering

iJOE | eISSN: 2626-8493 | Vol. 20 No. 15 (2024) | OPEN ACCESS

https://doi.org/10.3991/ijoe.v20i15.50409

PAPER

A Hybrid Technique of Diagnosing Kidney Disorder Using Deep Neural Network

M. Poovayar Priya[1](✉), **M. Ezhilarasan**[2]

[1]Dept. of CSE, Puducherry Technological University, Puducherry, India

[2]Dept. of IT, Puducherry Technological University, Puducherry, India

kavipriya63@ptuniv.edu.in

ABSTRACT

The growing demand for renal alternative medical diagnostics is driven by their non-invasive, early, real-time, and painless characteristics. Early diagnosis of kidney disease is crucial, given its severity as a health issue. This paper introduces a novel method that integrates residual networks with long short-term memory (LSTM) through deep feature analysis. The LSTM network is employed to extract global features from the iris, such as Wolfflin nodules and lacunae. The Res-Net classification system is then used to distinguish between kidney and non-kidney diseases. Various image-processing techniques are applied to segment, enhance, and normalize the iris image while extracting its distinctive features. Experimental results show that our model achieves 95% accuracy in classifying kidney and non-kidney conditions based on iris analysis. Future work aims to predict additional diseases using a deep neural network applied to iris images.

KEYWORDS

feature extraction, iris enhancement, iris normalization, iris segmentation, kidney disease, residual network, long short-term memory (LSTM)

1 INTRODUCTION

The kidneys are vital organs responsible for eliminating numerous metabolic waste products through urinary secretion. The nephron, the smallest structural and functional unit of the kidney, plays a key role in this process. It produces urine through mechanisms of filtration, reabsorption, secretion, and excretion as it processes the blood supplied to it. These processes remove nitrogenous wastes, such as uric acid from nucleic acid metabolism and urea from protein catabolism [1]. Additionally, the kidneys contribute to maintaining homeostasis [2] throughout the body by regulating blood pressure, extracellular fluid volume, electrolyte concentrations, and acid-base balance. The kidneys perform these homeostatic functions independently and in coordination with other organs, particularly those of the endocrine system. This coordination is mediated by various endocrine hormones,

Poovayar Priya, M., Ezhilarasan, M. (2024). A Hybrid Technique of Diagnosing Kidney Disorder Using Deep Neural Network. *International Journal of Online and Biomedical Engineering (iJOE)*, 20(15), pp. 43–59. https://doi.org/10.3991/ijoe.v20i15.50409

Article submitted 2024-06-04. Revision uploaded 2024-08-26. Final acceptance 2024-08-26.

including atrial natriuretic peptide [3], renin [4], angiotensin II [5], aldosterone [6], and antidiuretic hormone [7].

Nephropathy, also known as kidney disease or renal illness, refers to conditions that affect the kidneys. Nephritis [8] is an inflammatory kidney disease that can manifest in various forms depending on the location of the inflammation, which can be identified through blood tests. Nephrosis [9], on the other hand, is a non-inflammatory kidney condition. Nephritis can lead to nephritic syndrome [10], while nephrosis can result in nephrotic syndrome. Chronic illnesses such as systemic lupus erythematosus [11], diabetes mellitus [12], and high blood pressure (hypertension) [13] can all lead to nephropathy. Specifically, diabetic nephropathy [14] is caused by diabetes mellitus, and hypertensive nephropathy [15] results from high blood pressure.

According to a study, renal failure accounted for 2.1% of all fatalities among individuals aged 15 to 69 between 2001 and 2003, with this percentage rising to 2.9% from 2010 to 2013 [16]. A World Health Organization (WHO) report published in 2018 estimated that 5–10 million individuals died due to urinary problems [17], highlighting the increasing prevalence of kidney-related illnesses.

Traditional medical procedures for identifying kidney issues include pathological indicators, blood or urine anomalies, imaging tests, and measuring the glomerular filtration rate (GFR) [18]. The most accurate method for estimating GFR involves measuring the creatinine levels in the blood and urine. However, kidney failure is often exacerbated by patient financial difficulties, delayed diagnosis, and a lack of access to skilled medical professionals, particularly in rural areas. Early detection of renal disease is crucial for reducing morbidity and mortality rates.

Early diagnosis and alternative medicine are becoming increasingly important in future healthcare technology. Utilizing alternative pre-diagnostic techniques can help reduce costs, prevent complications, and address delays in diagnosis. One such alternative diagnostic method is iridology, also known as iris analysis. Iridology categorizes the human iris based on the body's organs, where marks, spots, or patterns in specific iris regions correspond to the health or dysfunction of particular organs.

For instance, abnormalities in the area around the pupil may indicate stomach issues, while kidney problems are often reflected at the bottom edge of the iris. The right iris is associated with the organs on the right side of the body, and the left iris corresponds to the organs on the left side [19]. Figure 1 illustrates the iridology chart with the human iris, which maps the left and right iris regions corresponding to kidney health.

In the proposed work, we develop a long short-term memory (LSTM)-based Res-Net model utilizing iridology for the early prediction of kidney problems. This method performs a general pre-diagnosis of kidney disease by analysing iris images, leveraging an iridology chart as a reference. The algorithm is executed on a supercomputer equipped with GPUs to ensure efficient processing. This analysis helps estimate the extent of kidney damage in humans. The system has been tested on 1,000 iris images (500 left and 500 right iris) and has achieved an accuracy of 95%.

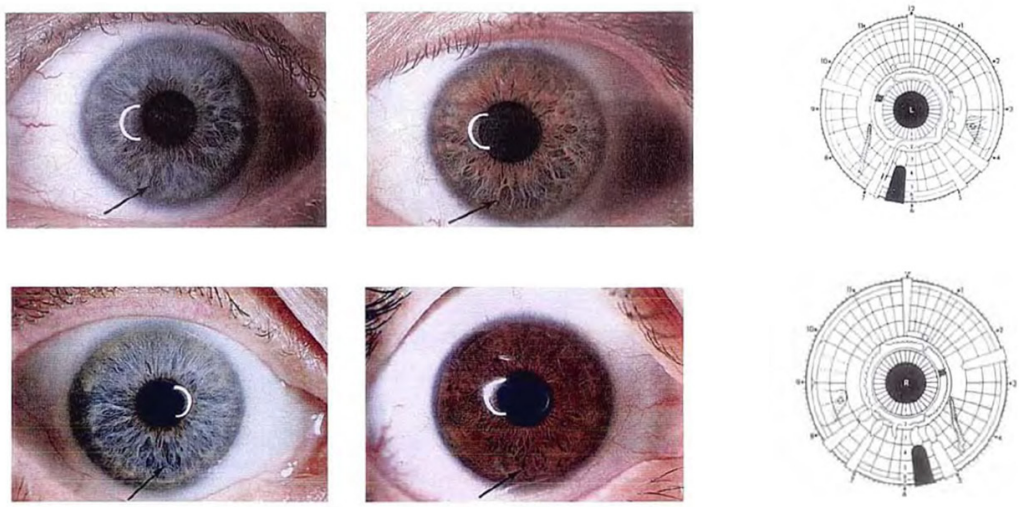

Fig. 1. Iridology chart of left and right iris

2 LITERATURE SURVEY

Various classifications based on deep learning methods have been implemented for image classification in recent years.

Naeem A.B. et al. explored the potential of integrating sensor data with artificial neural networks (ANNs) to enhance the early detection of heart disease [20]. By leveraging various sensors, such as ECG and PPG, crucial physiological data can be collected and analysed. Through advanced feature extraction techniques, relevant indicators such as heart rate variability and waveform patterns are derived from the sensor data. These features are then fed into an ANN model, specifically designed to identify patterns associated with heart disease. The ANN's ability to learn from large datasets enables it to distinguish between healthy and at-risk individuals with high accuracy. This approach not only offers a non-invasive, real-time solution for monitoring heart health but also promises to improve early diagnosis, thereby facilitating timely intervention and reducing the overall burden of heart disease.

To address the challenge of automatically identifying oral disease in white-light smartphone photos, Eman Shawky Mira [21] provided an easy-to-use yet effective image-collection and resampling approach that leverages deep learning algorithms. We use our collection of photos from five different sickness categories to test the latest HRNet, which was pre-trained on ImageNet. The results demonstrate that our methods can greatly improve smartphone photography image prediction ability for early cancer diagnosis. Kailash Kumar [22] focuses on creating a hybrid fuzzy deep neural network model for early-stage CKD prediction. This model is then assessed and compared to the existing radioimmunoassay technique. The findings demonstrate that the suggested model performs better at accurately identifying diseases than the current approach.

A model for deep learning The MobileNetV2 architecture served as the foundation for TL-MobileNetV2. The suggested model by Yonis Gulzar [23] was trained and tested on a dataset of 40 different fruit varieties. To increase the model's accuracy and efficiency, the MobileNetV2 architecture's classification layer was removed,

and five more layers were added to the TL-MobileNetV2 model. Future research will improve a mobile application by incorporating a greater variety of fruits to expand the scope of fruit classification. People with little experience will find this program useful in learning how to categorize various fruit species. Additionally, the dataset will be used to train various CNN models, and the outcomes will be compared to determine which model fits the data the best in terms of efficiency and accuracy.

An innovative end-to-end, pixel-by-pixel fully convolutional spatial propagation network (FCSPN) for HIS classification was proposed by Yenan Jiang [24]. Contextual spatial information modelling fails because traditional CNN models use convolutions with local receptive fields. A 3D fully convolution network (3D-FCN) and a convolutional spatial propagation network (CSPN) make up the FCSPN approach, which addresses this. It consists of two parts: first, HIS characteristics are extracted in an end-to-end pipeline using a preliminary classification algorithm based on 3D-FCN. When compared to the state-of-the-art methods now in use, the suggested FCSPN demonstrated superior performance.

AHF-Net, a unique adaptive hybrid fusion network, was created by Wenping Ma [25] for multi-resolution remote sensing picture classification. The primary obstacle in this discipline is figuring out how to effectively process the data and extract features to increase classification accuracy. Data fusion and feature fusion are the two components of this strategy. An adaptive weighted intensity-hue-saturation (AWIHS) technique was suggested for the data fusion section. A correlation-based attention feature fusion (CAFF) module was suggested for the feature fusion section. The suggested method's efficacy has been confirmed by experiments conducted on multiple datasets. However, there are still certain drawbacks to this approach: it is not a comprehensive foundation for classification, and the variations produced by AWIHS could influence further classifications.

An end-to-end fully convolutional segmentation network (FCSN) was proposed by Hao Sun [26]. The spatial land-cover distributions of cropped HSI cubes are typically difficult to recover with the current method. Whereas FCSN aims to categorize every pixel in an HSI cube, CNN-based techniques concentrate on identifying the cube's centre pixel. To categorize every pixel in an HSI cube at once, the proposed FCSN simultaneously investigates spatial land-cover distributions and spectral fingerprints. This approach, which has strong generalization potential, focuses on completely utilizing the spatial land-cover distributions of HSIs for categorization. Semi-supervised segmentation will be used in the future to investigate labelled and unlabelled pixels for HSI categorization.

A multitask deep learning system that simultaneously performs reconstruction and classification in an open world where unknown classes can exist was proposed by Shengjie Liu [27]. Experiments showed that, in comparison to state-of-the-art approaches, the suggested strategy greatly improves classification accuracy. The suggested approach will be very helpful in increasing classification accuracy and rejecting unknown classes. To achieve better categorization in the real world, more research focuses on applying skew-normal distribution, Gaussian distribution, and other distributions.

A polarimetric scattering information-based adaptive fuzzy super pixels (AFS) technique for PoISAR image classification was proposed by Yuwei Guo [28]. There are two problems: First, there is ineffective utilization of the polarimetric scattering information. Second, each image in the current approaches has a set fraction of unknown pixels. Creating a super pixel model and assessing AFS performance are the main goals of a straightforward classification procedure. Future research will

combine the AFS algorithm with a particular categorization technique to provide results that are more accurate.

An asynchronous contrastive learning-based technique known as the "Push and Pull Network (P2Net)" was introduced by Jianqi Chen [29]. Unbalanced fineness and imbalanced appearance are two difficult occurrences. In the "push-out stage" and "pull-in stage" of this approach, input photos are first decollated with one another before being combined into subclasses. The subclasses can be separated using this network, simplifying the classification process. With this approach, every network component may be trained end-to-end without the need for additional annotations.

A hyper-spectral categorization framework based on generative networks and combined channel-space attention mechanisms was presented by Weitao Chen [30] (JAGAN). The field of hyper-spectral remote sensing classification faces a number of challenges, such as the requirement to increase the accuracy of land cover classification with small sample sizes and the absence of hyper-spectral datasets for particular complex scenarios. The JAGAN model, which is based on the channel-spatial joint attention mechanism and GAN, was developed in order to efficiently extract more advantageous spatial and spectral information from hyper-spectral images. The findings showed that the suggested model concentrates on the important characteristics and then uses the joint attention module to give those features greater weights. It also obtains helpful features related to the current output and produces better identifiable feature representations for various categories.

To categorize multi-sensory data, Xu Liu et al. [31] developed a unique classification technique dubbed the deep multi-view union learning network (DMULN). Multisource image classification in the context of visual interpretation has emerged as a major issue for the current approach. In order to handle the multisource picture classification job, this technique proposes a DMULN, which addresses the problems associated with multi-view feature extraction and fusion. Results from the fusion categorization of multisource distant data are more trustworthy and useful. They will develop a more resilient multisource image categorization model in the future.

A linear programming incremental learning classifier (LPILC), which was suggested by Jing Bai et al. [32], can help deep learning classification models that are already in use adjust to new datasets. This approach can quickly and efficiently in terms of computations adjust to a new type of HSI data. According to extensive testing, when given the same data access and processing resources, the LPILC converges fastest and achieves the highest accuracy. Incorporating the suggested LPILC into more complex classification models in order to quickly update the model with a small amount of data.

For PAN and MS pictures, Xu Liu et al. [33] introduced a unique classification technique dubbed the deep group spatial-spectral attention fusion network. This method was presented to solve the PAN and MS image classification task in order to address the HR fusion classification problem. By mining the properties of pertinent data, this approach seeks to improve classification performance. The two primary components of the suggested approach are feature extraction and fusion. The suggested yields outcomes with greater accuracy. Because feature extraction and fusion are so versatile, the suggested technique can be used in a wide range of applications. It can also be updated over time, thanks to adaptive groups.

The multi-scale convolutional neural network with an autoencoder regularization joint contextual attention network (MCAR-CAN) is a novel SAR classification

algorithm that Zitong Wu [34] suggested. The autoencoder branch and the context attention branch make up this method's two branches. Since the decoder regularizes the encoder, asymmetric structure in the autoencoder branch can help the network become more focused on learning categorization information. By generating an attention weight related context correlation in the attention branch, attention mechanisms get stable and effective properties. A post-processing approach called Markov random field (MRF) is intended to increase the precision of categorization. Better robustness and learning capacity were demonstrated by the suggested algorithm. The classification accuracy is somewhat increased by the post-processing method and mixed strategy.

A unique unified deep learning network that uses both labelled and unlabelled input for training was proposed by Wei Wei [35]. Since pixel labelling is challenging and expensive in real-hyper-spectral image classification applications, the labels obtained inside an HSI are always limited and noisy, which leads to overfitting of the deep learning-based approach. The basic feature extraction module in the proposed network is shared by both the supervised clustering task and the conventional classification tasks. Additionally, a feature fusion module is designed to further fuse the high-level features from two tasks for improved feature representation. The outcomes demonstrated the suggested method's outstanding effectiveness, particularly in cases where the label is noisy and limited.

To classify SAR image scenes, Xiaoxue Qian [36] suggested a hybrid network that combined data-based and model-based techniques. It is challenging to obtain labelled samples for synthetic aperture radar (SAR) images using the current technology. The suggested approach uses a hybrid network called GCVAE-CNN, which combines CNN and GCVAE for SAR image scene classification with a small number of labelled samples. End-to-end generation and categorization are achieved by the hybrid network that combines model-based and data-based techniques. In further work, unique generation models will be built to increase the variety of samples produced, and unique CNNs will be designed to enhance the hybrid network's performance.

Qingji Guan [37] suggested using a two-branch architecture called ConsultNet to learn discriminative features. The suggested approach attempts to address the issues of various diseases present and irrelevant regions influencing the classification of chest X-ray images. The suggested approach performs better and beats the baseline in quantitative terms. In the future, think of annotating a small amount of the lesion region using ground truth, which would solve the problem of illness recognition through saliency detection.

A unique modality-specific attention network (MSAN) for multi-modal retinal image classification was proposed by Xingxin He [38]. The primary function of the attention mechanism is to suppress irrelevant data and draw attention to the discriminative area of the feature map. To represent modality-specific information from fundus and OCT pictures, two subnets are built. The modality-specific features are then fused to classify various retinal disorders. The suggested approach lowers clinic errors while streamlining workflow. In the future, correlations between various eye diseases will be considered to further enhance the performance of multi-disease retinal image classification. Additionally, self-supervised learning will be used to attempt learning visual features to concentrate on ROI in an unsupervised manner.

The paper focuses on developing an advanced machine-learning model for the segmentation of Alzheimer's disease (AD) using a Swin transformer-based architecture [39]. The goal is to improve the accuracy and efficiency of AD diagnosis by

integrating sophisticated techniques in image segmentation and feature fusion. The Swin transformer is employed for its ability to handle large-scale visual data with high accuracy. It's known for its efficiency in capturing global context and local details, which are crucial for medical image analysis. The segmentation module likely uses the Swin transformer to delineate regions of interest in brain images that may indicate the presence of Alzheimer's disease. The multi-scale Feature Pyramid Fusion module combines features from different scales to capture both fine and coarse details of the brain structures. This fusion helps in creating a more comprehensive and accurate model for detecting pathological changes associated with Alzheimer's disease.

From the literature survey, a significant challenge identified is overfitting, where the model performs well on training data but fails to generalize effectively to new, unseen data. This reduces its overall accuracy and reliability. Additionally, the annotation process for training data is time-consuming and labour-intensive, as it demands precise and consistent labelling of iris features. Furthermore, training models are complicated by the need for a complex multi-resolution architecture, which is essential to capture and process the intricate details of the iris accurately.

3 METHODS

This section contains the dataset used for implementation, iris segmentation, enhancement, normalization, feature extraction, and classification of kidney or non-kidney disease.

3.1 Dataset

Iris images were gathered using a Mobile-Eyes™ sensor, a product of L-1 Identify Solutions, across two sessions. The patient database consists of 1000 iris images, with 500 left and 500 right images taken in and around Puducherry hospitals and clinics. During image capture, patients were asked if they wore contact lenses, and this information was recorded. Images were captured using near-infrared (NIR) light, producing SVGA images with a width of 752 × 480 at a rate of 30 frames per second. The device features dual-iris enrolment, allowing simultaneous auto-capture of both the left and right eyes. It operates effectively in both dim and bright lighting conditions. The captured images are saved in PNG format with a resolution of 640 × 480.

The Mobile-Eyes™ sensors are powered by the Iris Analysis Software SDK, which includes modules for focus measurement, image segmentation, encoding, and scoring. During the capture process, patients were positioned about 5 cm from the scanner, and images were taken under standard room lighting conditions. To avoid occlusions, patients were instructed to keep their eyes wide open. The SDK's image assessment scoring module ensures that only images exceeding a predetermined evaluation score are stored or captured.

3.2 Iris segmentation

The acquired eye image was used to segment the iris, using Iris U-Net architecture [40]. The Iris U-Net architecture processes 572 × 572 input images and is

structured with five layers. It leverages Skip connections and detailed localization for enhanced performance. Skip connections link the encoder and decoder layers, merging high-resolution encoder features with up sampled decoder features. This design retains spatial information and improves pixel-level prediction accuracy. Additionally, the Iris U-Net achieves precise localization by integrating low-level and high-level data, which is critical for tasks such as medical imaging where minute details are essential. The architecture consists of three main components: the up sampling path (decoder) for high-resolution reconstruction, the down sampling path (encoder) for capturing contextual information, and the bottleneck layer that facilitates feature integration between the encoder and decoder. This structure enables accurate segmentation as shown in Figure 2 and effective context capture.

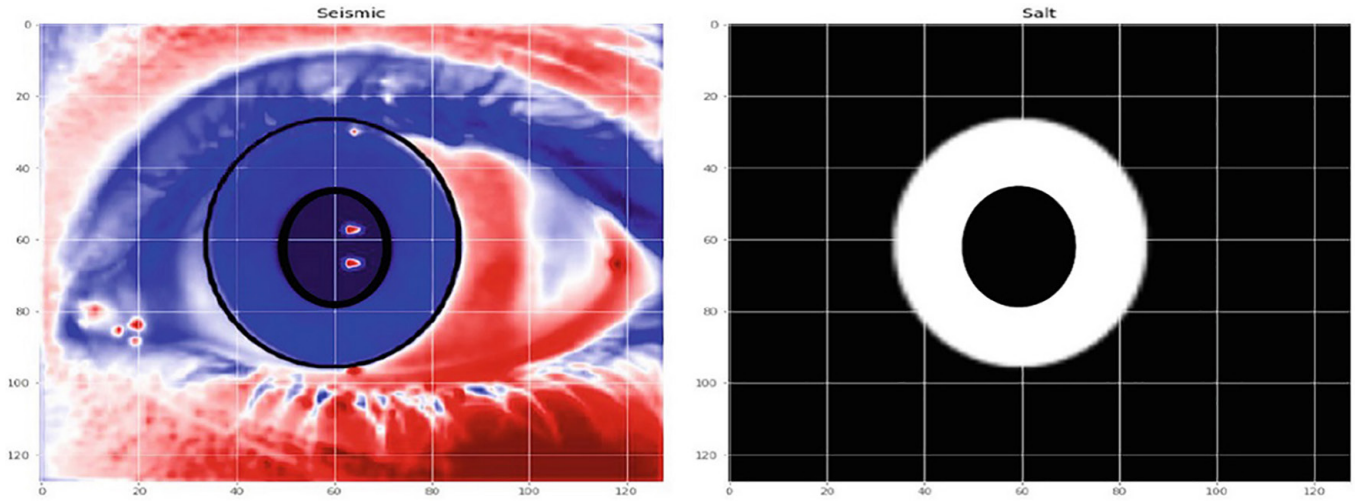

Fig. 2. Iris segmentation

3.3 Iris enhancement

The input to the enhancement process is the segmented iris from the segmentation stage. Iris-CS improves global details by enhancing contrast in small regions, making finer features more visible. It also controls the extent of contrast amplification to minimize the risk of noise enhancement. Additionally, Iris-CS refines local details by addressing illumination inconsistencies, which is especially beneficial for images with strong shadows and highlights. By normalizing illumination without significantly amplifying noise, Iris-CS helps maintain the natural appearance of the image as shown in Figure 3 while reducing blurriness.

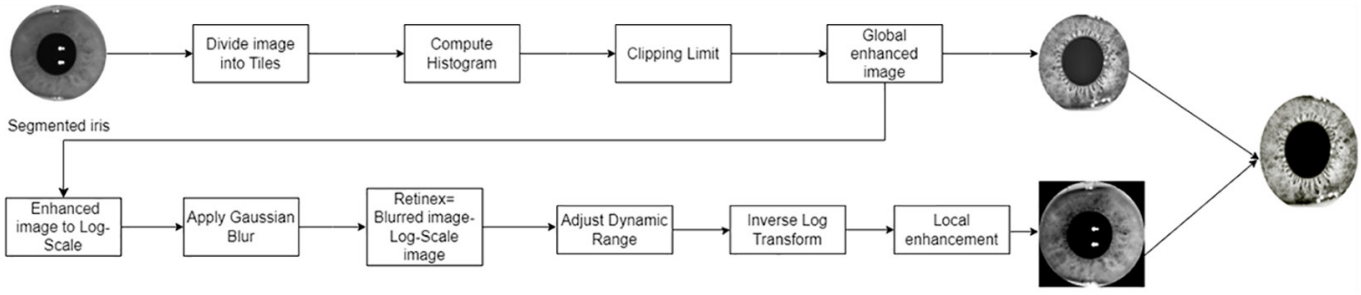

Fig. 3. Iris-CS model

3.4 Iris normalization

During the normalization procedure, the iris area is adjusted to standardized dimensions. Variations such as head tilt, camera rotation, eye rotation, and image distance can also affect dilation. An effective normalization technique should produce consistent dimensions for the same iris types across different conditions and distinct regions for different iris types under the same conditions. Daugman's rubber-sheet model explains this process by mapping each point in the iris region to polar coordinates (r, θ) as illustrated in Figure 4.

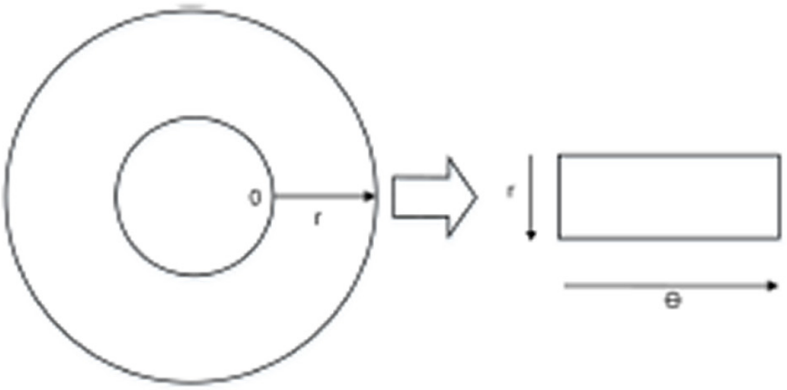

Fig. 4. Iris normalization

3.5 Feature extraction

Feature extraction techniques are employed to identify kidney disease in the iris by focusing on specific features such as lacunae and Wolfflin nodules. These features are extracted using LSTM layers within the network model. LSTM layers consist of memory cells that retain and update features over time steps. These memory cells store and manage important features from past inputs, which are crucial for making predictions at the current time step.

The gate mechanism in LSTM layers controls the flow of new features into the memory cell. It determines which features from the current input should be preserved in the memory cell. The cell state, which runs throughout the entire sequence, is adjusted by these gates and serves as a conveyor belt, enabling features to flow while maintaining long-term dependencies. The hidden state of an LSTM layer, the output at each time step, captures the relevant features learned from the input sequence and is used for predictions or passed to subsequent layers in the neural network, as shown in Figure 5. From each location in the iris image, pertinent features are extracted. These features include attributes such as the size, shape, intensity, texture, and spatial arrangement of the spots. In iris imaging, lacunae and Wolfflin nodules are effectively retrieved and characterized using these techniques.

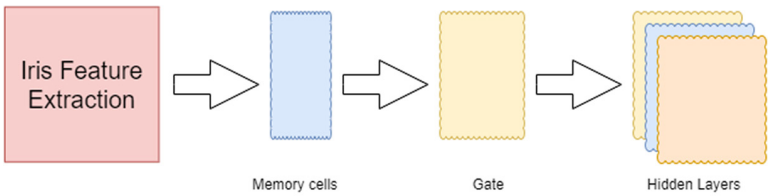

Fig. 5. LSTM layers for feature extraction

3.6 Analysis of kidney disease

Once the features are extracted, the classification system detects kidney disease using a residual network with LSTM features. Figure 6 illustrates this deep neural network architecture. This architecture splits the dataset into *k* subsets and trains the model *k* times, each time using a different subset as the validation set and the remaining *k*–1 subsets as the training set. This helps reduce the risk of overfitting. This architecture uses a combination of labelled and unlabelled data to reduce the annotation burden. It also starts training with lower-resolution images and progressively increases the resolution as the model learns to handle the data better.

The process begins with the image entering the input layer. In this architecture, a one-dimensional convolutional layer is used, with the number of features after reshaping denoted as $X_{\text{reshaped. shape [1]}}$, representing the expected input for the layer. The convolutional layer starts with a kernel size of seven and 64 filters to extract features from the data. Each convolutional layer is followed by batch normalization, which normalizes the layer's activations. A key feature of this architecture is the use of residual blocks. These blocks include skip connections, or shortcut connections, that apply batch normalization to each of the two convolutional layers in the block before adding the original input to their outputs. This design allows gradients to flow through the network without interruption, resolving the vanishing gradient problem. After each residual block, a max-pooling layer is used to reduce the spatial dimensions of the features.

The global average pooling layer simplifies each feature map to a single value by averaging all its values. This process reduces the spatial dimensions to 1×1, producing a fixed-length vector independent of the input size. The output from the global average pooling layer then passes through a dense layer with 256 units and ReLU activation. To mitigate overfitting, a dropout layer with a dropout rate of 0.5 is included.

Finally, a dense layer with a single unit and sigmoid activation performs binary classification, distinguishing between kidney and non-kidney conditions. The model, which uses the Adam optimizer and binary cross-entropy loss function, is trained on the entire dataset with a predefined batch size and number of epochs. This design, incorporating residual blocks, helps overcome the overfitting problem, annotation burden, and complex architecture and enhances performance on challenging tasks.

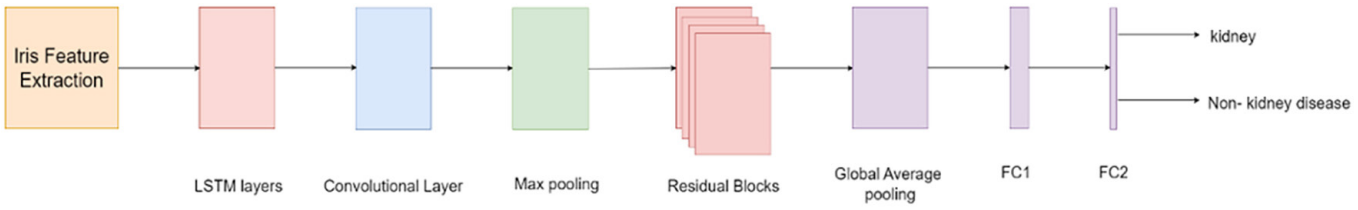

Fig. 6. Fusion of LSTM with Res-Net

4 RESULTS AND DISCUSSION

This section discusses the experimental analysis of left and right iris with a classification report and confusion matrix. It also compares the existing methods with the proposed method.

4.1 Evaluation of left iris

In the classification report shown in Figure 7, both classes (non-kidney and kidney) have a precision, recall, and F1-score, indicating that the model makes some errors in predicting either class. The accuracy, macro average, and weighted average indicate the classification performance across all metrics. Overall, this classification report suggests that the model performs exceptionally well on the entire dataset, achieving classification for both classes.

The curve shown in Figure 8 illustrates the trade-off between the true positive rate and the false positive rate for both classes.

True positive rate (TPR): For each class, TPR represents the proportion of correctly classified instances of that class among all actual instances of that class.

False positive rate (FPR): For each class, FPR represents the proportion of incorrectly classified instances of the opposite class among all actual instances of the opposite class.

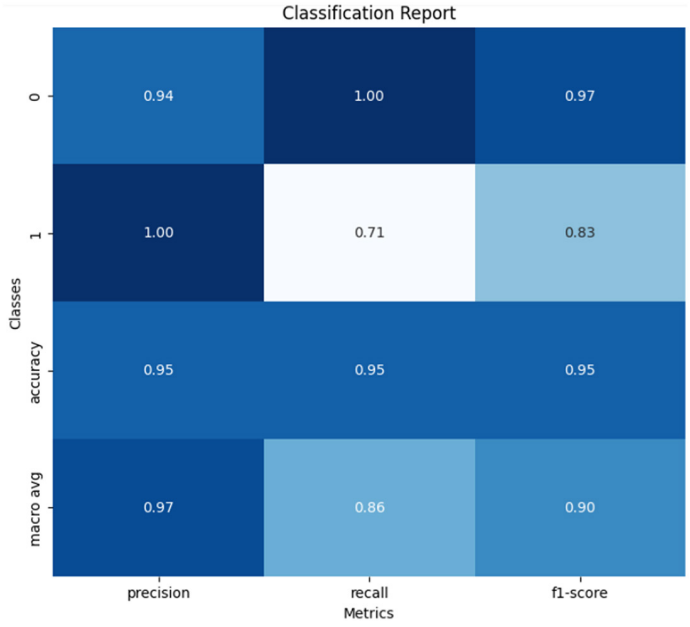

Fig. 7. Classification report of left iris

Mathematically, TPR and FPR for each class are calculated as:
For kidney class:

$$TPR\ kidney = \frac{TP\ kidney}{TP\ kidney + FN\ kidney}$$

$$FPR\ kidney = \frac{FP\ non\text{-}kidney}{FP\ non\text{-}kidney + TN\ non\text{-}kidney}$$

For non-kidney class:

$$TPR\ non\text{-}kidney = \frac{TP\ non\text{-}kidney}{TP\ non\text{-}kidney + FN\ non\text{-}kidney}$$

$$FPR\ non\text{-}kidney = \frac{FP\ kidney}{FP\ kidney + TN\ kidney}$$

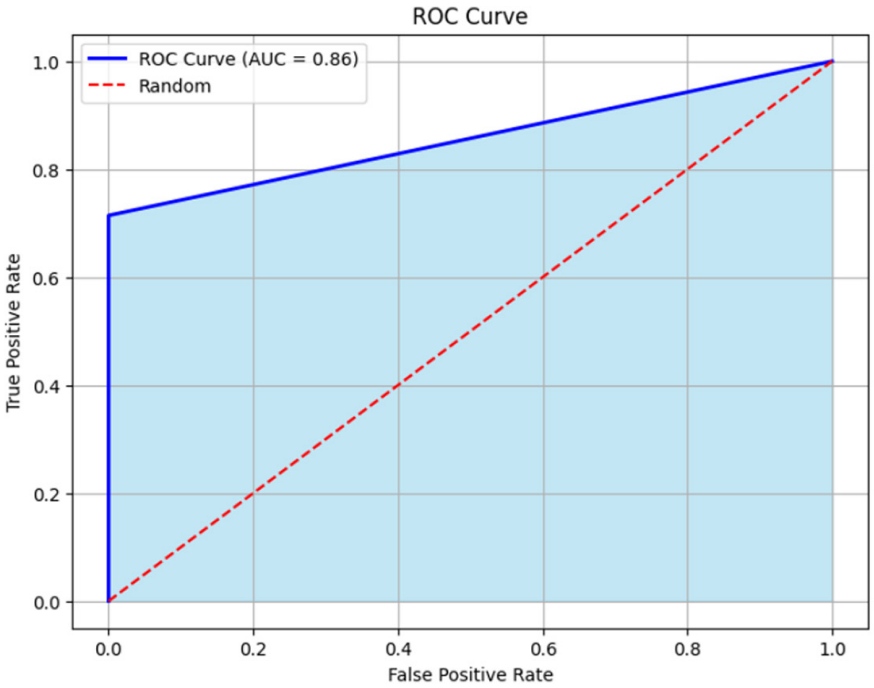

Fig. 8. ROC curve of left iris

4.2 Evaluation of right iris

In the classification report shown in Figure 9, both classes (non-kidney and kidney) have a precision, recall, and F1-score, indicating that the model makes some errors in predicting either class. The accuracy, macro average, and weighted average indicate classification performance across all metrics. Overall, this classification report suggests that the model performs exceptionally well on the entire dataset, achieving classification for both classes.

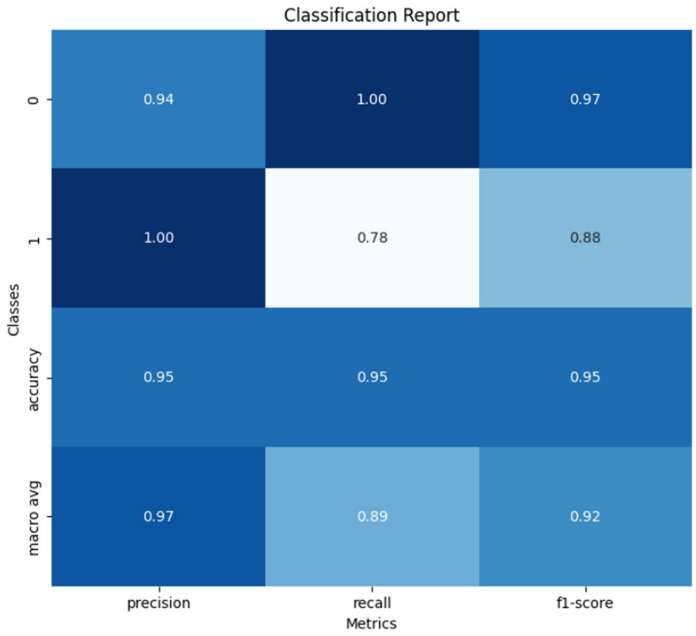

Fig. 9. Classification report of right iris

The curve shown in Figure 10 illustrates the trade-off between the true positive rate and the false positive rate for both classes.

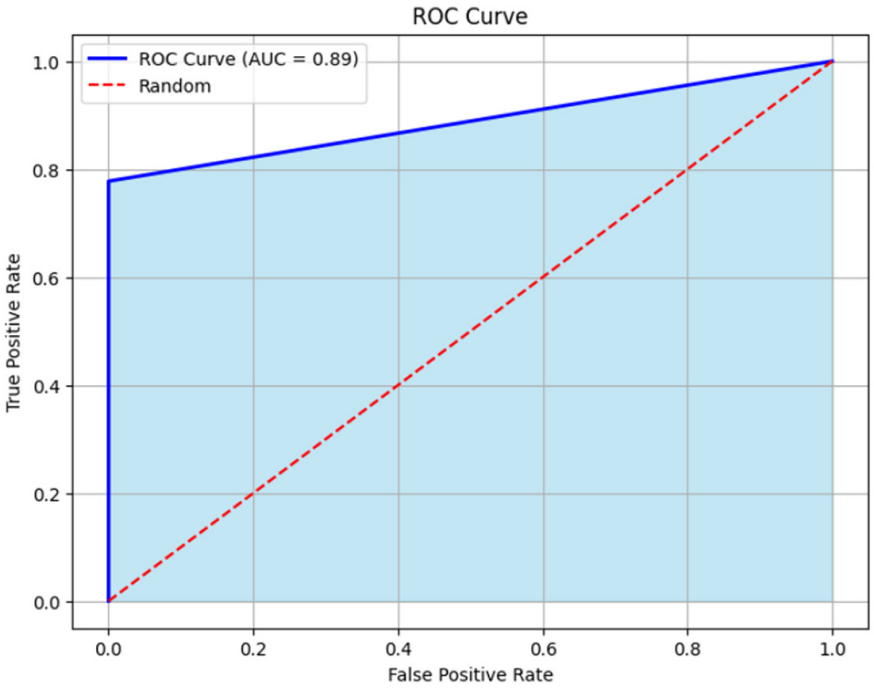

Fig. 10. ROC curve of right iris

4.3 Visualization and comparison with state-of-art-methods

Figure 11 visualizes the performance metrics of different models for predicting the "non-disease" class, "kidney" class, and accuracy metrics. Our proposed method achieves 95% accuracy in predicting kidney disease using iris analysis compared with state-of-the-art methods.

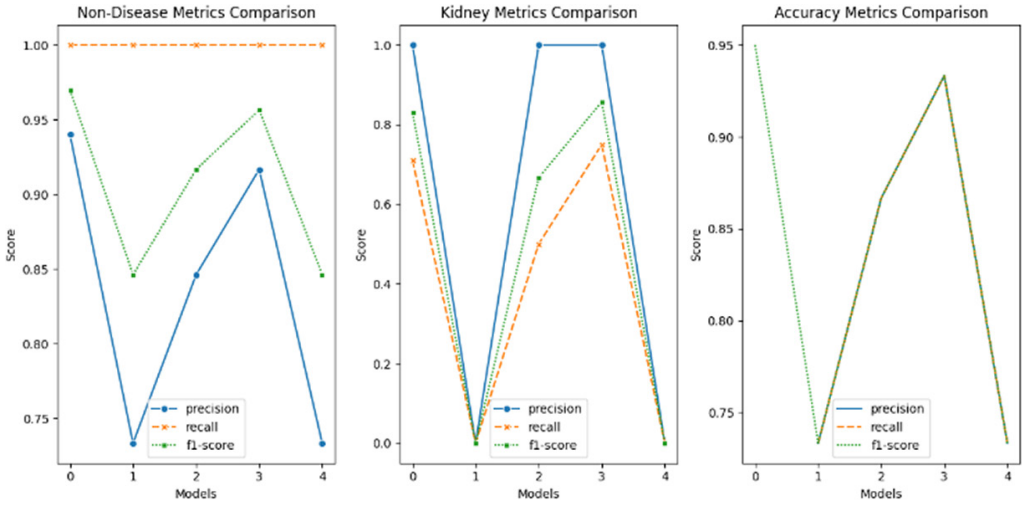

Fig. 11. Visualization result

As shown in Table 1, we compare our method with existing network models. The column "Authors" of Table 1 shows similar work that was done by the other

authors with different applications. The accuracy column shows the percentage of subjects classified through iris images and algorithms as kidney subjects. From Table 1, the results show that the proposed method has 95% accuracy compared with other methods. This indicates that the findings obtained are indeed effective and promising.

Table 1. Comparison with existing methods

S. No	Authors	Accuracy
1	Naeem A.B et al. [20]	86%
2	Mira E.S et al. [21]	92%
3	Kumar K et al. [22]	93%
4	Agarwal R et al. [23]	94.4%
5	Proposed Method	95%

5 CONCLUSION

In this study, we used an image-processing technique to detect the presence of kidney disease. Using the Iris U-Net model, we first separated the iris from eye images. Subsequently, an image enhancement approach was employed to improve the quality of the iris image. Then, features of the iris are extracted using an LSTM-based deep neural network. It extracts both deep features and high-level features. Our proposed framework classified the kidney and non-kidney of the iris images. By detecting kidney disease in the iris, the experimental results demonstrated an outperformance. Out of 1000 iris images in our datasets, the proposed model achieves 95% accuracy in predicting kidney disease. This paper focuses on the detection of kidney abnormalities, laying the groundwork for future research to identify the different stages of kidney disorders. By enhancing current detection methods, future investigations could develop more advanced diagnostic tools capable of not only recognizing kidney abnormalities but also classifying the progression of kidney diseases. This approach would significantly improve early diagnosis, treatment planning, and patient outcomes by enabling healthcare providers to intervene at the most appropriate stage of the disease.

6 REFERENCES

[1] C. J. Lote, *Principles of Renal Physiology*, 5th Edition. New York, NY: Springer, 2012. https://doi.org/10.1007/978-1-4614-3785-7

[2] H. Koeslag Johan, T. Saunders Peter, and A. Wessels Jabus, "The chromogranins and counter-regulatory hormones: Do they make homeostatic sense?" *Journal of Physiology*, vol. 517, no. 3, pp. 643–649, 1999. https://doi.org/10.1111/j.1469-7793.1999.0643s.x

[3] J. Venugopal, "Pharmacological modulation of the natriuretic peptide system," *Expert Opinion on Therapeutic Patents*, vol. 13, no. 9, pp. 1389–1409, 2003. https://doi.org/10.1517/13543776.13.9.1389

[4] G. Nguyen, "Renin, (pro)renin and receptor: An update," *Clinical Science (London)*, vol. 120, no. 5, pp. 169–178, 2011. https://doi.org/10.1042/CS20100432

[5] H. Lu, L. A. Cassis, C. W. Kooi, and A. Daugherty, "Structure and functions of angiotensinogen," *Hypertension Research*, vol. 39, pp. 492–500, 2016. https://doi.org/10.1038/hr.2016.17

[6] M. Ducher *et al.*, "Aldosterone-to-renin ratio for diagnosing aldosterone-producing adenoma: A multicentre study," *Archives of Cardiovascular Diseases*, vol. 105, no. 12, pp. 623–630, 2012. https://doi.org/10.1016/j.acvd.2012.07.006

[7] G. P. Mavani, M. V. DeVita, and M. F. Michelis, "A review of the nonpressor and nonantidiuretic actions of the hormone vasopressin," *Frontiers in Medicine*, vol. 2, 2015. https://doi.org/10.3389/fmed.2015.00019

[8] P. Pokhrel *et al.*, "Unusual presentations in systemic lupus erythematosus with concurrent IgA nephropathy lesion: A rare case report from Eastern Nepal," *Annals of Medicine and Surgery*, vol. 86, no. 10, pp. 6140–6144, 2024. https://doi.org/10.1097/MS9.0000000000002401

[9] S. A. Alenazi, "Incidence and pathological patterns of nephrotic syndrome among infants and children: A systematic review," *Cureus*, vol. 16, no. 4, p. e58331, 2024. https://doi.org/10.7759/cureus.58331

[10] A. Gigante *et al.*, "Changes in renal microcirculation in patients with nephrotic and nephritic syndrome: The role of the resistive index," *Microvascular Research*, vol. 152, p. 104641, 2024. https://doi.org/10.1016/j.mvr.2023.104641

[11] J. Law, C. Sorrento, and A. Saxena, "Vaccination updates and special considerations for systemic lupus erythematosus patients," *Current Opinion in Rheumatology*, vol. 36, no. 2, pp. 148–153, 2024. https://doi.org/10.1097/BOR.0000000000000992

[12] Z. I. Saydaxmedov and U. I. Mahmudov, "Diabetes mellitus and covid-19; a bidirectional interplay," *Formation of Psychology and Pedagogy as Interdisciplinary Sciences*, vol. 2, no. 25, pp. 130–136, 2024.

[13] K. Sabapathy *et al.*, "Prevalence of hypertension and high-normal blood pressure among young adults in Zimbabwe: Findings from a large, cross-sectional population-based survey," *The Lancet Child & Adolescent Health*, vol. 8, no. 2, pp. 101–111, 2024. https://doi.org/10.1016/S2352-4642(23)00287-0

[14] J. Wu, K. Li, M. Zhou, H. Gao, W. Wang, and W. Xiao, "Natural compounds improve diabetic nephropathy by regulating the TLR4 signaling pathway," *Journal of Pharmaceutical Analysis*, vol. 14, no. 8, p. 100946, 2024. https://doi.org/10.1016/j.jpha.2024.01.014

[15] F. Ozdemir *et al.*, "Autosomal dominant kidney disease phenocopying hypertensive nephropathy in Turkish cypriot families," *Research Square*, 2024. https://doi.org/10.21203/rs.3.rs-2844330/v2

[16] A. V. Mulay, "Renal failure deaths in India: Crying for attention," *The National Medical Journal of India*, vol. 30, no. 3, pp. 148–149, 2017.

[17] P. Ellis, "The global burden of kidney disease," *Journal of Kidney Care*, vol. 5, no. 2, pp. 102–102, 2020. https://doi.org/10.12968/jokc.2020.5.2.102

[18] L. A. Stevens and A. S. Levey, "Measured GFR as a confirmatory test for estimated GFR," *Journal of the American Society of Nephrology*, vol. 20, no. 11, pp. 2305–2313, 2009. https://doi.org/10.1681/ASN.2009020171

[19] B. Jensen, *Iridology Simplified*, Escondido, CA: Author, 1980.

[20] A. B. Naeem *et al.*, "Heart disease detection using feature extraction and artificial neural networks: A sensor-based approach," *IEEE Access*, vol. 12, pp. 37349–37362, 2024. https://doi.org/10.1109/ACCESS.2024.3373646

[21] E. S. Mira *et al.*, "Early diagnosis of oral cancer using image processing and artificial intelligence," *Fusion: Practice and Applications*, vol. 14, no. 1, pp. 293–308, 2024. https://doi.org/10.54216/FPA.140122

[22] K. Kumar, M. Pradeepa, M. Mahdal, S. Verma, M. V. L. N. RajaRao, and J. V. N. Ramesh, "A deep learning approach for kidney disease recognition and prediction through image processing," *Applied Sciences*, vol. 13, no. 6, p. 3621, 2023. https://doi.org/10.3390/app13063621

[23] R. Agarwal, P. Samant, A. Bansal, and R. Agarwal, "Artificial intelligence for iris-based diagnosis in healthcare," in *Handbook of Metrology and Applications*, D. K. Aswal, S. Yadav, T. Takatsuji, P. Rachakonda, and H. Kumar, Eds., pp. 1–31, 2023. https://doi.org/10.1007/978-981-19-1550-5_106-1

[24] Y. Jiang, Y. Li, S. Zou, H. Zhang, and Y. Bai, "Hyperspectral image classification with spatial consistence using fully convolutional spatial propagation network," *IEEE Transactions on Geoscience and Remote Sensing*, vol. 59, no. 12, pp. 10425–10437, 2021. https://doi.org/10.1109/TGRS.2021.3049282

[25] W. Ma *et al.*, "A novel adaptive hybrid fusion network for multiresolution remote sensing images classification," *IEEE Transactions on Geoscience and Remote Sensing*, vol. 60, pp. 1–17, 2021. https://doi.org/10.1109/TGRS.2021.3062142

[26] H. Sun, X. Zheng, and X. Lu, "A supervised segmentation network for hyperspectral image classification," *IEEE Transactions on Image Processing*, vol. 30, pp. 2810–2825, 2021. https://doi.org/10.1109/TIP.2021.3055613

[27] S. Liu, Q. Shi, and L. Zhang, "Few-shot hyperspectral image classification with unknown classes using multitask deep learning," *IEEE Transactions on Geoscience and Remote Sensing*, vol. 59, no. 6, pp. 5085–5102, 2021. https://doi.org/10.1109/TGRS.2020.3018879

[28] Y. Guo, L. Jiao, S. Wang, S. Wang, F. Liu, and W. Hua, "Fuzzy superpixels for polarimetric SAR images classification," *IEEE Transactions on Fuzzy Systems*, vol. 26, no. 5, pp. 2846–2860, 2018. https://doi.org/10.1109/TFUZZ.2018.2814591

[29] J. Chen, K. Chen, H. Chen, W. Li, Z. Zou, and Z. Shi, "Contrastive learning for fine-grained ship classification in remote sensing images," *IEEE Transactions on Geoscience and Remote Sensing*, vol. 60, pp. 1–16, 2022. https://doi.org/10.1109/TGRS.2022.3192256

[30] W. Chen, S. Ouyang, J. Yang, X. Li, G. Zhou, and L. Wang, "JAGAN: A framework for complex land cover classification using Gaofen-5 AHSI images," *IEEE Journal of Selected Topics in Applied Earth Observations and Remote Sensing*, vol. 15, pp. 1591–1603, 2022. https://doi.org/10.1109/JSTARS.2022.3144339

[31] X. Liu *et al.*, "Deep multiview union learning network for multisource image classification," *IEEE Transactions on Cybernetics*, vol. 52, no. 6, pp. 4534–4546, 2020. https://doi.org/10.1109/tcyb.2020.3029787

[32] J. Bai *et al.*, "Class incremental learning with few-shots based on linear programming for hyperspectral image classification," *IEEE Transactions on Cybernetics*, vol. 52, no. 6, pp. 5474–5485, 2020. https://doi.org/10.1109/tcyb.2020.3032958

[33] X. Liu, L. Li, F. Liu, B. Hou, S. Yang, and L. Jiao, "GAFNet: Group attention fusion network for PAN and MS image high-resolution classification," *IEEE Transactions on Cybernetics*, vol. 52, no. 10, pp. 10556–10569, 2021. https://doi.org/10.1109/TCYB.2021.3064571

[34] Z. Wu, B. Hou, and L. Jiao, "Multiscale CNN with autoencoder regularization joint contextual attention network for SAR image classification," *IEEE Transactions on Geoscience and Remote Sensing*, vol. 59, no. 2, pp. 1200–1213, 2021. https://doi.org/10.1109/TGRS.2020.3004911

[35] W. Wei, S. Xu, L. Zhang, J. Zhang, and Y. Zhang, "Boosting hyperspectral image classification with unsupervised feature learning," *IEEE Transactions on Geoscience and Remote Sensing*, vol. 60, pp. 1–15, 2021. https://doi.org/10.1109/TGRS.2021.3054037

[36] X. Qian *et al.*, "A hybrid network with structural constraints for SAR image scene classification," *IEEE Transactions on Geoscience and Remote Sensing*, vol. 60, pp. 1–17, 2021. https://doi.org/10.1109/TGRS.2021.3059742

[37] Q. Guan, Y. Huang, Y. Luo, P. Liu, M. Xu, and Y. Yang, "Discriminative feature learning for thorax disease classification in chest X-ray images," *IEEE Transactions on Image Processing*, vol. 30, pp. 2476–2487, 2021. https://doi.org/10.1109/TIP.2021.3052711

[38] X. He, Y. Deng, L. Fang, and Q. Peng, "Multi-modal retinal image classification with modality-specific attention network," *IEEE Transactions on Medical Imaging*, vol. 40, no. 6, pp. 1591–1602, 2021. https://doi.org/10.1109/TMI.2021.3059956

[39] N. Gharaibeh, A. A. Abu-Ein, O. M. Al-Hazaimeh, K. M. O. Nahar, W. A. Abu-Ain, and M. M. Al-Nawashi, "Swin transformer-based segmentation and multi-scale feature pyramid fusion module for alzheimer's disease with machine learning," *International Journal of Online & Biomedical Engineering (iJOE)*, vol. 19, no. 4, pp. 22–50, 2023. https://doi.org/10.3991/ijoe.v19i04.37677

[40] M. P. Priya and M. Ezhilarasan, "IRIS Segmentation technique using IRIS-UNet method," in *Proceedings of Advanced Concepts for Intelligent Vision Systems: 21st International Conference,* ACIVS 2023 Kumamoto, Japan, 2023.

7 AUTHORS

M. Poovayar Priya did B.Tech. from the Pondicherry Engineering College, in 2016, and the M.Tech. from SRM University, in 2018. She is currently a Research Scholar at Puducherry Technological University. She has authored more than three papers published in international conferences and professional journals. Her research interests include deep learning, image processing, neural networks, and artificial intelligence (E-mail: kavipriya63@ptuniv.edu.in).

M. Ezhilarasan did B.Tech. and M.Tech. from Pondicherry University, Puducherry, in 1990 and 1996, respectively, and the Ph.D. degree from Pondicherry Engineering College, Puducherry, in 2007. He is a Professor in the Department of IT, at Puducherry Technological University (formerly Pondicherry Engineering College), India. He has more than 70 publications in international journals. He has presented more than 50 papers at international conferences. He has guided both UG and PG candidate's projects. His research interests include multimedia coding, multi-biometrics, image processing, machine and deep learning.